

Adaptive Graph Auto-Encoder for General Data Clustering

Xuelong Li, Hongyuan Zhang, Rui Zhang

School of Computer Science and Center for OPTical IMagery Analysis and Learning (OPTIMAL),
Northwestern Polytechnical University, Xian 710072, Shaanxi, P. R. China
xuelong_li@ieee.org, hyzhang98@gmail.com, ruizhang8633@gmail.com

Abstract

Graph-based clustering plays an important role in the clustering area. Recent studies about graph convolution neural networks have achieved impressive success on graph type data. However, in general clustering tasks, the graph structure of data does not exist such that the strategy to construct a graph is crucial for performance. Therefore, how to extend graph convolution networks into general clustering tasks is an attractive problem. In this paper, we propose a graph auto-encoder with local structure-preserving for general data clustering, which constructs the graph adaptively. The adaptive process is designed to utilize the non-Euclidean structure sufficiently. We further design a novel mechanism to avoid the collapse caused by the adaptive construction. Via combining the generative model for network embedding and graph-based clustering, a graph auto-encoder with a novel decoder is developed such that it performs well in weighted graph used scenarios. Extensive experiments prove the superiority of our model.

Introduction

Clustering, which intends to group data points without any prior information, is one of the most fundamental tasks in machine learning. As well as the well-known k -means, graph-based clustering (Ng, Jordan, and Weiss 2002; Nie, Wang, and Huang 2014; Zhang et al. 2018) is also a representative kind of clustering method. Graph-based clustering methods can capture manifold information so that they are available for the non-Euclidean type data, which is not provided by k -means. Therefore, they are widely used in practice. Due to the success of deep learning, how to combine neural networks and traditional clustering models has been studied a lot (Shaham et al. 2018; Xie, Girshick, and Farhadi 2016; Zhang et al. 2019). In particular, CNN-based clustering models have been extensively investigated (Yang, Parikh, and Batra 2016; Ghasedi Dizaji et al. 2017; Yang et al. 2019). However, the convolution operation may be unavailable on other kinds of datasets, *e.g.*, text datasets, social network datasets, *etc.*

Network embedding is a fundamental task for graph type data such as recommendation systems, social networks, *etc.*

The goal is to map nodes of a given graph into latent features (namely embedding) such that the learned embedding can be utilized on node classification, node clustering, and link prediction. Roughly speaking, the network embedding approaches can be classified into 2 categories: generative models (Wang et al. 2018; Perozzi, Al-Rfou, and Skiena 2014; Grover and Leskovec 2016) and discriminative models (Cao, Lu, and Xu 2016; Wang, Cui, and Zhu 2016). The former tries to model a connectivity distribution for each node while the latter learns to distinguish whether an edge exists between two nodes directly.

In recent years, graph neural networks (*GNN*) (Scarselli et al. 2008), especially graph convolution neural networks (*GCN*), have attracted a mass of attention due to the success made in the neural networks area. *GNNs* extend classical neural networks into irregular data so that the deep information hidden in graphs is exploited sufficiently. In this paper, we only focus on *GCNs* and its variants. *GCNs* have shown superiority compared with traditional network embedding models. Similarly, graph auto-encoder (*GAE*) (Kipf and Welling 2016) is developed to extend *GCN* into unsupervised learning.

However, the existing methods are limited to graph type data while no graph is provided for general data clustering. Since a large proportion of clustering methods are based on the graph, it is reasonable to consider how to employ *GCN* to promote the performance of graph-based clustering methods. In this paper, we propose an Adaptive Graph Auto-Encoder to extend graph auto-encoder into common scenarios. The main contributions are listed as follows:

- To build a desirable graph, our model incorporates generative models of network embedding. The learned connectivity distribution is also used as the goal that graph auto-encoder aims to reconstruct.
- Our model updates the graph adaptively according to the generated embedding such that it can exploit the deep information and revise the poor graph caused by raw features. We eliminate the collapse caused by the adaptive construction via changing the sparsity of the graph. Besides, the related theoretical analyses are given to understand the collapse phenomenon.
- Our model also employs a manifold regularization to preserve the local structure, which can be regarded as pseudo-supervised information.

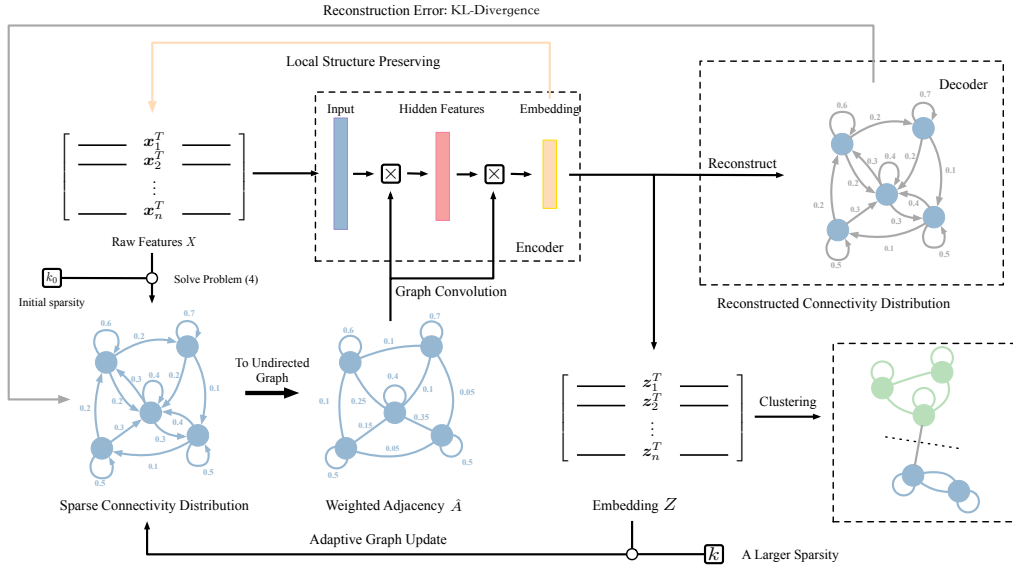


Figure 1: Framework of AdaGAE. k_0 is the initial sparsity. First, we construct a sparse graph via the generative model defined in Eq. (4). The learned graph is employed to apply the GAE designed for the weighted graphs. After training the GAE, we update the graph from the learned embedding with a larger sparsity, k . With the new graph, we re-train the GAE. These steps are repeated until the convergence.

Preliminary and Related Work

Notations

In this paper, matrices and vectors are represented by uppercase and lowercase letters respectively. A graph is represented as $\mathcal{G} = (\mathcal{V}, \mathcal{E}, \mathcal{W})$ and $|\cdot|$ is the size of some set. Vectors whose all elements equal 1 are represented as **1**. If $\langle v_i, v_j \rangle \in \mathcal{E}$, then $\mathcal{W}_{ij} > 0$; otherwise, $\mathcal{W}_{ij} = 0$. For every node $v_i \in \mathcal{V}$, it is represented by a d -dimension vector x_i and thus, \mathcal{V} can be also denoted by $X = [x_1, x_2, \dots, x_n]^T \in \mathbb{R}^{n \times d}$. The amount of data points and clusters are represented as n and c respectively. All proofs are shown in supplementary.

Deep Clustering

An important topic in clustering field is deep clustering, which utilize the neural network to enhance the capacity of model. A fundamental model is auto-encoder (AE) (Hinton and Salakhutdinov 2006), which has been widely used in diverse clustering methods (Makhzani et al. 2015; Xie, Girshick, and Farhadi 2016; Peng et al. 2018; Zhang et al. 2019). Besides the AE-based models, Spectral-Net (Shaham et al. 2018) attempts to transform the core idea of spectral clustering to neural networks. In image clustering fields, CNN-based models have achieved impressive performance. For instance, JULE (Yang, Parikh, and Batra 2016) employs both CNN and RNN to obtain better representation. DEPICT (Ghasedi Dizaji et al. 2017) and deep spectral clustering with dual networks (Yang et al. 2019) are based on convolution auto-encoders such that they can only be applied on image clustering.

Graph Auto-Encoder

In recent years, GCNs have been studied a lot to extend neural networks to graph type data. How to design a graph convolution operator is a key issue and has attracted a mass of attention. Most of them can be classified into 2 categories, spectral methods (Niepert, Ahmed, and Kutzkov 2016) and spatial methods(Bruna et al. 2013) . In this paper, we focus on a simple but widely used convolution operator (Kipf and Welling 2017), which can be regarded as both the spectral operator and spatial operator. Formally, if the input of a graph convolution layer is $X \in \mathbb{R}^{n \times d}$ and the adjacency matrix is A , then the output is defined as

$$H = \varphi(\hat{A}XW), \quad (1)$$

where $\varphi(\cdot)$ is certain activation function, $\hat{A} = \tilde{D}^{-\frac{1}{2}} \tilde{A} \tilde{D}^{-\frac{1}{2}}$, $\tilde{A} = A + I$, \tilde{D} denotes the degree matrix ($\tilde{D}_{ii} = \sum_{j=1}^n \tilde{A}_{ij}$), and W denotes the parameters of GCN. It should be pointed out that \tilde{A} is a graph with self-loop for each node and \hat{A} is the normalized adjacency matrix. More importantly, $\hat{A}X$ is equivalent to compute weighted means for each node with its first-order neighbors from the spatial aspect. To improve the performance, MixHop (Abu-El-Haija et al. 2019) aims to mix information from different order neighbors and SGC (Wu et al. 2019) tries to utilize higher-order neighbors. The capacity of GCN is also proved to some extent (Xu et al. 2019). GCN and its variants are usually used on semi-supervised learning. Besides, since the training of each GCN layer needs all data to finish a complete propagation, several models are proposed to speed it up (Chen, Zhu, and Song 2018; Chiang et al. 2019).

To apply graph convolution on unsupervised learning, GAE is proposed (Kipf and Welling 2016). GAE firstly

transforms each node into latent representation (namely embedding), which is similar to GCN, and then aims to reconstruct some part of the input. GAEs proposed in (Kipf and Welling 2016; Pan et al. 2018; Wang et al. 2019) intend to reconstruct the adjacency via decoder while GAEs developed in (Wang et al. 2017) attempt to reconstruct the content. The difference is which extra mechanism (such as attention, adversarial learning, graph sharpness, etc.) is used.

Proposed Model

In this section, we will show the proposed model, Adaptive Graph Auto-Encoder (*AdaGAE*) for general data clustering. The core idea is illustrated in Figure 1.

Probabilistic Perspective of Weighted Graphs

In this paper, the underlying connectivity distribution of node v_i is denoted by conditional probability $p(v|v_i)$ such that $\sum_{j=1}^n p(v_j|v_i) = 1$. From this perspective, a link can be regarded as a sampling result according to $p(v|v_i)$, which is the core assumption of the generative network embedding.

In general clustering scenarios, links between two nodes frequently do not exist. Therefore, we need to construct a weighted graph via some scheme. Since $p(v_j|v_i) \geq 0$, the probability can be regarded as valid weights. Note that $p(v_j|v_i) \neq p(v_i|v_j)$ usually holds, and therefore, the constructed graph should be viewed as a directed graph. Therefore, the construction of the weighted graph is equivalent to finding the underlying connectivity distribution. Given differences among samples $\{d_{ij}\}_{i,j=1}^n$, we expect that

$$\min_{p(\cdot|v_i)} \sum_{i=1}^n \mathbb{E}_{v_j \sim p(\cdot|v_i)} d_{ij} = \sum_{i=1}^n \sum_{j=1}^n p(v_j|v_i) \cdot d_{ij}, \quad (2)$$

such that the constructed graph is locally coherent. However, it is impracticable to solve the above problem directly, as it has a trivial solution: $p(v_i|v_i) = 1$ and $p(v_j|v_i) = 0$ if $j \neq i$. A universal method is to employ *Regularization Loss Minimization*, and the objective is given as

$$\min_{p(\cdot|v_i)} \sum_{i=1}^n \mathbb{E}_{v_j \sim p(\cdot|v_i)} d_{ij} + \mathcal{R}(p(\cdot|v_i)), \quad (3)$$

where $\mathcal{R}(\cdot)$ is some regularization term. Usually, the difference d_{ij} is measured by the Euclidean distance. In most practical situations, although the global distance is usually unreliable, the local distance (Roweis and Saul 2000; He and Niyogi 2004; Tenenbaum, Silva, and Langford 2000) is frequently regarded as a vital part in manifold learning. Similarly, an ideal distribution should be sparse so that it can ignore the significantly different nodes. From another aspect, a graph is usually sparse and thus, $p(v|v_i)$ should be 0 for most nodes. Formally, let $\mathbf{p}_i = [p(v_1|v_i), p(v_2|v_i), \dots, p(v_n|v_i)]$ and the sparse distribution should satisfy that $\|\mathbf{p}_i\|_0 \leq s$ where s represents a small integer. Hence, the regularization term should be $\gamma\|\mathbf{p}_i\|_0$. Nevertheless, ℓ_0 -norm is non-convex and it is NP-hard to solve. Generally, we try to solve a convex ℓ_1 relaxation problem, i.e., $\mathcal{R}(p(\cdot|v_i)) = \gamma\|\mathbf{p}_i\|_1$, since

ℓ_1 -norm is the tightest convex relaxation of ℓ_0 -norm and it guarantees the sparseness of solution. However, the sparsity degree cannot be controlled precisely, i.e., we need to tune the trade-off parameter γ manually. Theorem shows that the ℓ_2 -norm relaxation can guarantee steerable sparsity. To control sparsity of distribution for each node, we utilize point-wise regularization.

Theorem 1. *The ℓ_2 -norm relaxation of problem (3),*

$$\min_{p(\cdot|v_i)} \sum_{i=1}^n \mathbb{E}_{v_j \sim p(\cdot|v_i)} d_{ij} + \gamma_i \|\mathbf{p}_i\|_2^2, \quad (4)$$

has a k -sparse solution if γ_i satisfies

$$\frac{1}{2}(kd_i^{(k)} - \sum_{v=1}^k d_i^{(v)}) < \gamma_i \leq \frac{1}{2}(kd_i^{(k+1)} - \sum_{v=1}^k d_i^{(v)}). \quad (5)$$

where $d_i^{(v)}$ denotes the v -th smallest value of $\{d_{ij}\}_{j=1}^n$.

The point-wise regularization can control the sparsity of each node but also increase the amount of hyper-parameters. In this paper, we simply choose an identical sparsity for all nodes. Formally, γ_i is set as the upper bound for all nodes,

$$\gamma_i = \frac{1}{2}(kd_i^{(k+1)} - \sum_{v=1}^k d_i^{(v)}). \quad (6)$$

It should be emphasized that there is only one hyper-parameter, sparsity k , in our model, which is much easier to tune than the traditional ℓ_1 relaxation method. More importantly, we will show that problem (4) can be solved analytically.

Optimization To keep notations uncluttered, $p(v_j|v_i)$ is simplified as p_{ij} . Then the problem (4) is equivalent to solve the following subproblem individually

$$\min_{\mathbf{p}_i^T \mathbf{1} = 1, \mathbf{p}_i \geq 0} \sum_{j=1}^n p_{ij} d_{ij} + \gamma_i \|\mathbf{p}_i\|_2^2. \quad (7)$$

To keep the discussion more concise, the subscript i is neglected. Due to d_j is constant, we have

$$\min_{\mathbf{p}^T \mathbf{1} = 1, \mathbf{p} \geq 0} \sum_{j=1}^n p_j d_j + \gamma \|\mathbf{p}\|_2^2 \Leftrightarrow \min_{\mathbf{p}^T \mathbf{1} = 1, \mathbf{p} \geq 0} \|\mathbf{p} + \frac{\mathbf{d}}{2\gamma}\|_2^2. \quad (8)$$

Then the Lagrangian of the above equation is

$$\mathcal{L} = \|\mathbf{p} + \frac{\mathbf{d}}{2\gamma}\|_2^2 + \alpha(1 - \sum_{j=1}^n p_j) + \sum_{j=1}^n \beta_j(-p_j), \quad (9)$$

where α and β_j are the Lagrange multipliers. According to the KKT conditions, we have

$$\begin{cases} p_j + \frac{d_j}{2\gamma} - \alpha - \beta_j = 0 \\ \beta_j p_j = 0, \beta_j \geq 0 \\ \sum_{j=1}^n p_j = 1, p_j \geq 0 \end{cases} \Rightarrow p_j = (\alpha - \frac{d_j}{2\gamma})_+, \quad (10)$$

where $(\cdot)_+ = \max(\cdot, 0)$. Without loss of generality, suppose that $d_1 \leq d_2 \leq \dots \leq d_n$. According to Theorem, $\|\mathbf{p}\|_0 =$

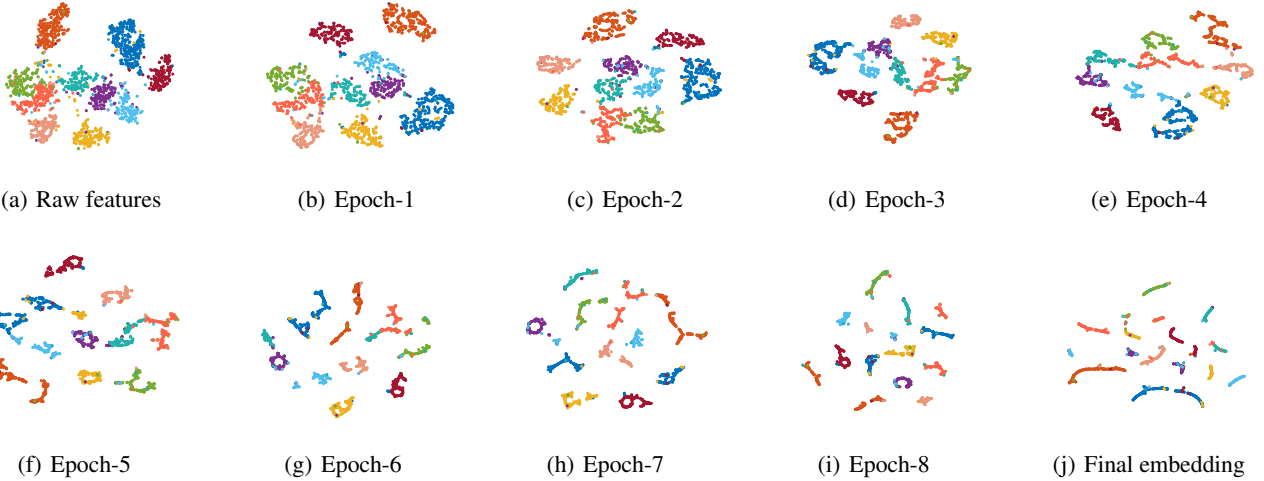


Figure 2: Visualization of the learning process of AdaGAE on USPS. Figure (b)-(i) show the embedding learned by AdaGAE at the i -th epoch, while the raw features and the final results are shown in Figure (a) and (j), respectively. An epoch corresponds to an update of the graph (given in Eq. (12)).

Algorithm 1 Algorithm to optimize AdaGAE

Require: Initial sparsity k_0 , the increment of sparsity t and number of iterations to update weight adjacency T .

$$Z = X, k = k_0.$$

for $i = 1, 2, \dots, T$ **do**

 Compute γ_i via Eq. (6).

 Compute $d_{ij} = \|z_i - z_j\|_2^2$.

 Compute $p(\cdot|v_i)$ and \hat{A} by solving problem (4) with k .

repeat

 Update GAE with Eq. (16) by the gradient descent.

until convergence or exceeding maximum iterations.

 Get new embedding Z .

$$k = k + t.$$

end for

 Perform spectral clustering on \hat{A} , or run k -means on Z .

Ensure: Clustering assignments.

k , or equivalently, $\alpha - \frac{d_{k+1}}{2\gamma} \leq 0 < \alpha - \frac{d_k}{2\gamma}$ where $k \in [1, n]$.

Due to $p^T \mathbf{1} = 1$, we have

$$\alpha = \frac{1}{k} \left(1 + \sum_{j=1}^k \frac{d_j}{2\gamma} \right). \quad (11)$$

Substitute Eq. (6) into Eq. (11), and we have

$$p_j = \left(\frac{d_{k+1} - d_j}{\sum_{j=1}^k (d_{k+1} - d_j)} \right)_+. \quad (12)$$

If $k \geq n$, then it is not hard to verify that Eq. (12) is also the optima. Accordingly, the connectivity distribution can be calculated via closed-form solutions.

Graph Auto-Encoder for Weighted Graph

After obtaining the connectivity distribution by solving problem (4), we transform the directed graph to an undirected graph via $\mathcal{W}_{ij} = (p(v_i|v_j) + p(v_j|v_i))/2$, and the

connectivity distribution serves as the reconstruction goal of graph auto-encoder, which will be elaborated soon.

Encoder As shown in (Kipf and Welling 2017), graphs with self-loops show better performance, *i.e.*, $\tilde{A} = A + I$. Due to $d_{ii} = 0$, $p(v_i|v_i) \in (0, 1)$ if $k > 1$. Particularly, the weights of self-loops are learned adaptively rather than the primitive I . Consequently, we can simply set $\tilde{A} = \mathcal{W}$ and $\hat{A} = \tilde{D}^{-\frac{1}{2}} \tilde{A} \tilde{D}^{-\frac{1}{2}}$. The encoder consists of multiple GCN layers and aims to transform raw features to latent features with the constructed graph structure. Specifically speaking, the latent feature generated by m layers is defined as

$$Z = \varphi_m(\hat{A} \varphi_{m-1}(\dots \varphi_1(\hat{A} X W_1) \dots) W_m). \quad (13)$$

Decoder Instead of reconstructing the weight matrix \tilde{A} , we aim to recover the connectivity distribution $p(v|v_i)$. Firstly, distances of latent features Z are calculated by $\hat{d}_{ij} = \|z_i - z_j\|_2^2$. Secondly, the connectivity distribution is reconstructed by a normalization step

$$q(v_j|v_i) = \frac{\exp(-\hat{d}_{ij})}{\sum_{j=1}^n \exp(-\hat{d}_{ij})}. \quad (14)$$

The above process can be regarded as inputting $-\hat{d}_{ij}$ into a SoftMax layer. Clearly, as \hat{d}_{ij} is smaller, $q(v_j|v_i)$ is larger. In other words, the similarity is measured by Euclidean distances rather than inner-products, which are usually used in GAE. To measure the difference between two distributions, Kullback-Leibler (KL) Divergence is therefore utilized and the objective function is defined as

$$\min_{q(\cdot|v_i)} KL(p\|q) \Leftrightarrow \min_{q(\cdot|v_i)} \sum_{i,j=1}^n p(v_j|v_i) \log \frac{1}{q(v_j|v_i)} \quad (15)$$

Note that it is equivalent to minimize the cross entropy, which is widely employed in classification tasks.

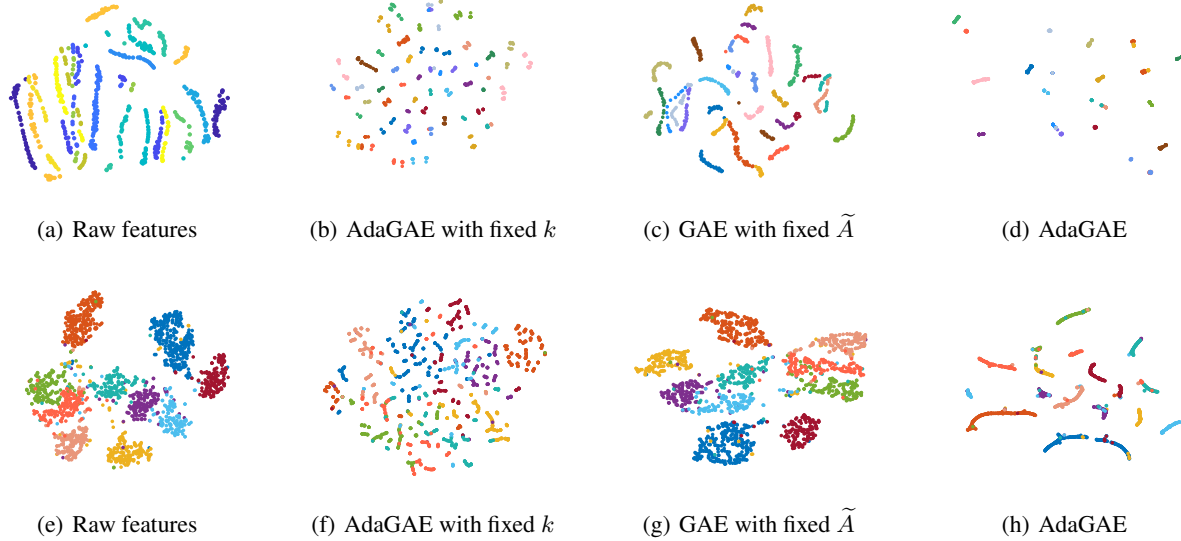


Figure 3: t-SNE visualization on UMIST and USPS: The first line illustrates results on UMIST and the second line shows results on USPS. Clearly, AdaGAE projects most semblaible samples into the analogous embedding.

Local Structure-Preserving A primary drawback of auto-encoders is that there may exist diverse latent representation schemes that can be reconstructed well via the decoder due to the powerful representation capacity of neural networks. Nevertheless, some kinds of representations may be useless even harmful. To break this restriction, a popular method is to introduce some prior information such as adversarial auto-encoder (Makhzani et al. 2015) and variational auto-encoder (Kingma and Welling 2014). Since the similarities are measured by distances and local information is often credible (especially in manifold learning), we add a local structure-preserving penalty term into Eq. (15) and thus, the cost function is defined as

$$\begin{aligned} & \min_q \sum_{i,j=1}^n p(v_j|v_i) \log \frac{1}{q(v_j|v_i)} + \frac{\lambda}{2} \tilde{A}_{ij} \|z_i - z_j\|_2^2 \\ & \Leftrightarrow \min_q \sum_{i,j=1}^n p(v_j|v_i) \log \frac{1}{q(v_j|v_i)} + \lambda \text{tr}(Z \tilde{L} Z^T), \end{aligned} \quad (16)$$

where $\tilde{L} = \tilde{D} - \tilde{A}$ and λ is a tradeoff parameter to balance the cross entropy term and local consistency penalty term.

Adaptive Graph Auto-Encoder

In the last subsection, the weighted adjacency matrix is viewed as fixed during training. However, the weighted adjacency matrix is computed by optimizing Eq. (4). The whole clustering process should contain connectivity learning and hence, the weighted adjacency should be updated adaptively during training. A feasible approach is to recompute the connectivity distribution based on the embedding Z , which contains the potential manifold information of data. However, the following theorem shows that the simple update based on latent representations may lead to the collapse.

Theorem 2. Let $p^{(k)}(\cdot|v_i)$ be the k -smallest $p(\cdot|v_i)$ and $\hat{d}_{ij} = \|z_i - z_j\|_2$ where z_i is generated by GAE with sparsity k . If $|q(\cdot|v_i) - p(\cdot|v_i)| \leq \varepsilon$ and $p^{(k)}(\cdot|v_i) \geq \sqrt{\varepsilon}$, then the solution of $\min_{p(\cdot|v_i)} \sum_{i=1}^n \mathbb{E}_{v_j \sim p(\cdot|v_i)} \hat{d}_{ij} + \gamma_i \|p_i\|_2^2$, with the same sparsity, degenerates into a uniform distribution such that the weighted graph degenerates into an unweighted graph.

Intuitively, the unweighted graph is indeed a bad choice for clustering. Therefore, the update step with the same sparsity coefficient k may result in collapse. To address this problem, we assume that

Assumption 1. Suppose that the sparse and weighted adjacency contains sufficient information. Specifically, weights of edges are large if it is within a cluster, or small otherwise. Then, with latent representations, samples of an identical cluster become more cohesive measured by Euclidean distance.

According to the above assumption, samples from a cluster are more likely to lie in a local area after GAE mapping. Hence, the sparsity coefficient k increases when updating weight sparsity. The step size t which k increases with needs to be discussed. In an ideal situation, we can define the upper bound of k as

$$k_m^* = \min(|\mathcal{C}_1|, |\mathcal{C}_2|, \dots, |\mathcal{C}_c|), \quad (17)$$

where \mathcal{C}_i denotes the i -th cluster and $|\mathcal{C}_i|$ is the size of \mathcal{C}_i . Although $|\mathcal{C}_i|$ is not known, we can define k_m empirically to ensure $k_m \leq k_m^*$. For instance, k_m can be set as $\lfloor \frac{n}{c} \rfloor$ or $\lfloor \frac{n}{2c} \rfloor$. Accordingly, the step size $t = \frac{k_m - k_0}{T}$ where T is the number of iterations to update the weight adjacency.

To sum up, Algorithm 1 summarizes the whole process to optimize AdaGAE.

Table 1: ACC (%)

Methods	Text	20news	Isolet	Segment	PALM	UMIST	JAFFE	COIL20	USPS	MNIST
K-Means	86.34	25.26	59.11	54.97	70.39	42.87	72.39	58.26	64.67	55.87
CAN	50.31	25.39	61.47	49.13	88.10	69.62	96.71	84.10	67.96	74.85
RCut	53.44	28.06	65.96	43.23	61.36	61.31	83.62	69.57	63.86	63.52
NCut	55.34	31.26	60.06	51.74	61.19	60.05	80.44	70.28	63.50	64.90
DEC	50.62	25.11	34.17	14.29	27.45	36.47	62.95	74.35	42.30	81.22
DFKM	52.77	29.65	51.99	51.47	67.45	45.47	90.83	60.21	73.42	48.37
GAE	53.45	25.59	61.41	60.43	88.45	61.91	94.37	69.10	76.63	70.22
MGAE	50.48	41.47	46.31	50.44	51.47	49.19	87.22	60.99	64.13	55.17
GALA	50.31	28.16	53.59	49.57	79.45	41.39	94.37	80.00	67.64	74.26
GAE [†]	50.31	33.55	62.05	47.66	82.10	72.17	96.71	85.97	79.40	71.07
Method-A	50.00	38.54	66.15	41.13	88.30	73.22	96.71	92.43	67.48	73.87
Method-B	51.13	33.35	54.49	38.66	91.80	32.00	47.42	33.82	34.09	14.04
AdaGAE	89.31	77.28	66.22	60.95	95.25	83.48	97.27	93.75	91.96	92.88

Another Explanation of Degeneration Theorem 3 demonstrates that the SoftMax output layer with $-\hat{d}_{ij}$ is equivalent to solve problem (3) with a totally different regularization. Therefore, the perfect reconstruction may lead to bad performance.

Theorem 3. *The decoder of AdaGAE is equivalent to solve the following problem*

$$\min_{q(\cdot|v_i)} \sum_{i=1}^n \mathbb{E}_{v_j \sim q(\cdot|v_i)} \hat{d}_{ij} - H_i(v) \quad (18)$$

where $H_i(v) = -\sum_{j=1}^n q(v_j|v_i) \log q(v_j|v_i)$ represents the entropy of the connectivity distribution of node v_i .

Spectral Analysis

As mentioned in the above subsection, AdaGAE generates a weighted graph with adaptive self-loops. Analogous to SGC (Wu et al. 2019), Theorem 4 shows that adaptive self-loops also reduce the spectrum of the normalized Laplacian, *i.e.*, it smooths the Laplacian.

Theorem 4. *Let $\tilde{A}' = \tilde{A} - \text{diag}(\tilde{A})$ and $\hat{A}' = \tilde{D}'^{-\frac{1}{2}} \tilde{A}' \tilde{D}'^{-\frac{1}{2}}$. According to eigenvalue decomposition, suppose $I - \hat{A} = Q \Lambda Q^T$ and $I - \hat{A}' = Q' \Lambda' Q'^T$. The following inequality always holds*

$$0 = \lambda_1 = \lambda'_1 < \lambda_n < \lambda'_n \quad (19)$$

where λ_i and λ'_i denote the i -th smallest eigenvalue of $I - \hat{A}$ and $I - \hat{A}'$, respectively.

Computational Complexity

In the phase of training GCN, the most time-consuming operation is to compute $\hat{A}T_i$ where $T_i = XW_i \in \mathbb{R}^{n \times d_i}$. Since \hat{A} is sparse, the amount of non-zero entries is denoted by $|\mathcal{E}|$. Therefore, the computational complexity of each iteration to update GCN is $O(|\mathcal{E}|d_i)$. To construct and update the graph matrix, A , $O(n^2)$ time is required which is same with the spectral clustering. After the embedding is obtained, the complexity to get clustering assignments is $O(n^2c)$ (using the spectral clustering) or $O(ndc)$ (using k -means).

Experiments

In this section, details of AdaGAE are demonstrated and the results are shown. The visualization supports the theoretical analyses mentioned in the last section.

Datasets and Compared Methods

AdaGAE is evaluated on 10 datasets of different types, including 2 text datasets (*Text* and *20news*), 3 UCI (Dua and Graff 2017) datasets (*Isolet*, *Segment*, and *PALM*), and 5 image datasets (*UMIST* (Hou et al. 2013), *JAFFE* (Lyons, Budynek, and Akamatsu 1999), *COIL20* (Nene, Nayar, and Murase 1996), *USPS* (Hull 1994), and *MNIST-test* (LeCun)). Note that *USPS* used in our experiments is a subset with 1854 samples of the whole dataset. To keep notations simple, *MNIST* is denoted by *MNIST*.

To evaluate the performance of AdaGAE, 9 methods serve as competitors. To ensure the fairness, 4 clustering methods without neural networks are used, including *K-Means*, *CAN* (Nie, Wang, and Huang 2014), *Ratio Cut* (*RCut*) (Hagen and Kahng 1992), and *Normalized Cut* (*NCut*) (Ng, Jordan, and Weiss 2002). Two deep clustering for general data clustering, *DEC* (Xie, Girshick, and Farhadi 2016) and *DFKM* (Zhang et al. 2019), also serve as an important baseline. Besides, three GAE-based methods are used, including *GAE* (Kipf and Welling 2016), *MGAE* (Wang et al. 2017), and *GALA* (Park et al. 2019). All codes are downloaded from the homepages of authors. The concrete information of datasets and settings of competitors can be found in supplementary.

Experimental Setup

In our experiments, the encoder consists of two GCN layers. If the input dimension is 1024, the first layer has 256 neurons and the second layer has 64 neurons. Otherwise, the two layers have 128 neurons and 64 neurons respectively. The activation function of the first layer is set as ReLU while the other one employs the linear function. The initial sparsity k_0 is set as 5 and the upper bound k_m is searched from $\{\lfloor \frac{n}{c} \rfloor, \lfloor \frac{n}{2c} \rfloor\}$. The tradeoff coefficient λ is searched from

Table 2: NMI (%)

Methods	Text	20news	Isolet	Segment	PALM	UMIST	JAFFE	COIL20	USPS	MNIST
K-Means	<u>51.09</u>	0.27	74.15	55.40	89.98	65.47	80.90	74.58	62.88	54.17
CAN	2.09	3.41	78.17	52.62	<u>97.08</u>	<u>87.75</u>	<u>96.39</u>	<u>90.93</u>	<u>78.85</u>	77.30
RCut	0.35	4.59	<u>78.55</u>	53.22	85.78	77.64	90.63	84.16	70.35	70.29
NCut	0.93	4.57	72.11	51.11	85.21	77.54	89.56	84.70	70.43	72.15
DEC	2.09	0.27	70.13	0.00	55.22	56.96	82.83	90.37	48.71	<u>80.25</u>
DFKM	0.25	3.39	69.81	49.91	86.74	67.04	92.01	76.81	71.58	38.75
GAE	35.63	4.49	74.63	50.22	94.87	80.24	93.26	86.45	76.02	65.58
MGAE	1.40	<u>23.41</u>	65.06	39.26	81.13	68.00	89.65	73.59	62.18	57.33
GALA	2.09	3.09	71.60	<u>57.09</u>	89.50	63.71	92.54	87.71	71.50	75.65
GAE [†]	2.09	10.30	78.61	53.86	93.86	87.00	96.39	95.62	78.46	76.15
Method-A	0.52	25.18	79.76	52.16	96.96	87.04	96.39	97.26	76.45	76.59
Method-B	0.14	6.38	77.70	30.02	97.80	52.08	59.55	55.46	35.39	1.63
AdaGAE	51.59	49.60	78.89	59.76	98.18	91.03	96.78	98.36	84.81	85.31

$\{10^{-3}, 10^{-2}, \dots, 10^3\}$. The number of graph update step is set as 10 and the maximum iterations to optimize GAE varies in [150, 200].

To study the roles of different parts, the ablation experiments are conducted: GAE with $\lambda = 0$ and fixed \tilde{A} (denoted by GAE^{\dagger}), AdaGAE with fixed \tilde{A} (denoted by *Method-A*), and AdaGAE with fixed sparsity k (denoted by *Method-B*).

Two popular clustering metrics, the clustering accuracy (*ACC*) and normalized mutual information (*NMI*), are employed to evaluate the performance. All methods are run 10 times and the means are reported. The code of AdaGAE is implemented under pytorch-1.3.1 on a PC with a NVIDIA GeForce GTX 1660 GPU. The exact settings of all methods can be found in supplementary.

Experimental Results

To illustrate the process of AdaGAE, Figure 2 shows the learned embedding on USPS at the i -th epoch. An epoch means a complete training of GAE and an update of the graph. The maximum number of epochs, T , is set as 10. In other words, the graph is constructed 10 times. Clearly, the embedding becomes more cohesive with the update.

ACCs and NMIs of all methods are reported in Table 1 and 2. The best results of both competitors and AdaGAEs are highlighted in boldface while the suboptimal results are underlined. From Table 1 and 2, we conclude that:

- On text datasets (Text and 20news), most graph-based methods get a trivial result, as they group all samples into the same cluster such that NMIs approximate 0. Only k -means, MGAE, and AdaGAE obtain the non-trivial assignments.
- Classical clustering models work poorly on large scale datasets. Instead, DEC works better on the large scale datasets. Although GAE-based models (GAE, MGAE, and GALA) achieve impressive results on graph type datasets, they fail on the general datasets, which is probably caused by . In particular, AdaGAE is stable on all datasets due to the adaptive update of the graph.

- When the sparsity k keeps fixed, AdaGAE collapses on most of datasets. For example, ACC shrinks about 50% and NMI shrinks about 40% on COIL20.
- From the comparison of three extra experiments, we confirm that the adaptive graph update plays a positive role. Besides, the designed architecture of GAE for weighted graph improves the performance on most of datasets.

Besides, Figure 4 illustrates the learned embedding vividly. Combining with Theorem 2, if k is fixed as a constant, then \tilde{A} degenerates into an unweighted adjacency matrix and a cluster is broken into a mass of groups. Each group only contains a small number of data points and they scatter chaotically which leads to collapse. Instead, the adaptive process introduced above connects these groups before degeneration via increasing sparsity k , and hence, the embeddings in a cluster become cohesive. It should be emphasized that a large k_0 frequently leads to capture the wrong information. After the transformation of GAE, the nearest neighbors are more likely to belong with the same cluster and thus it is rational to increasing k_0 with an adequate step size.

Conclusion

In this paper, we propose a novel clustering model for general data clustering, namely Adaptive Graph Auto-Encoder (*AdaGAE*). Generative graph representation model is utilized to construct a weighted graph with steerable sparsity. To exploit potential information, we employ graph convolution operator and thus a graph auto-encoder with local structure-preserving is designed. More importantly, as the graph used in GAE is constructed artificially, an adaptive update step is developed to update the graph with the help of learned embedding. Related theoretical analyses demonstrate the reason why AdaGAE with fixed sparsity collapses in the update step. In experiments, we show the significant performance of AdaGAE and verify the effectiveness of the adaptive update step via the ablation experiments. Surprisingly, the visualization supports the theoretical analysis well and helps to understand how AdaGAE works.

References

Abu-El-Haija, S.; Perozzi, B.; Kapoor, A.; Alipourfard, N.; Lerman, K.; Harutyunyan, H.; Ver Steeg, G.; and Galstyan, A. 2019. MixHop: Higher-Order Graph Convolutional Architectures via Sparsified Neighborhood Mixing. In *International Conference on Machine Learning*, 21–29.

Bruna, J.; Zaremba, W.; Szlam, A.; and LeCun, Y. 2013. Spectral networks and locally connected networks on graphs. *arXiv preprint arXiv:1312.6203*.

Cao, S.; Lu, W.; and Xu, Q. 2016. Deep neural networks for learning graph representations. In *Thirtieth AAAI conference on artificial intelligence*.

Chen, J.; Zhu, J.; and Song, L. 2018. Stochastic Training of Graph Convolutional Networks with Variance Reduction. In *International Conference on Machine Learning*, 942–950.

Chiang, W.-L.; Liu, X.; Si, S.; Li, Y.; Bengio, S.; and Hsieh, C.-J. 2019. Cluster-gcn: An efficient algorithm for training deep and large graph convolutional networks. In *Proceedings of the 25th ACM SIGKDD International Conference on Knowledge Discovery & Data Mining*, 257–266.

Dua, D.; and Graff, C. 2017. UCI Machine Learning Repository. URL <http://archive.ics.uci.edu/ml>.

Ghasedi Dizaji, K.; Herandi, A.; Deng, C.; Cai, W.; and Huang, H. 2017. Deep clustering via joint convolutional autoencoder embedding and relative entropy minimization. In *Proceedings of the IEEE international conference on computer vision*, 5736–5745.

Grover, A.; and Leskovec, J. 2016. node2vec: Scalable feature learning for networks. In *Proceedings of the 22nd ACM SIGKDD international conference on Knowledge discovery and data mining*, 855–864.

Hagen, L.; and Kahng, A. B. 1992. New spectral methods for ratio cut partitioning and clustering. *IEEE transactions on computer-aided design of integrated circuits and systems* 11(9): 1074–1085.

He, X.; and Niyogi, P. 2004. Locality Preserving Projections. In *Advances in Neural Information Processing Systems* 16, 153–160.

Hinton, G. E.; and Salakhutdinov, R. 2006. Reducing the dimensionality of data with neural networks. *Science* 313(5786): 504–507.

Hou, C.; Nie, F.; Li, X.; Yi, D.; and Wu, Y. 2013. Joint embedding learning and sparse regression: A framework for unsupervised feature selection. *IEEE Transactions on Cybernetics* 44(6): 793–804.

Hull, J. 1994. A database for handwritten text recognition research. *IEEE Transactions on Pattern Analysis and Machine Intelligence* 16(5): 550–554.

Kingma, D. P.; and Welling, M. 2014. Auto-encoding Variational Bayes. In *ICLR*.

Kipf, T. N.; and Welling, M. 2016. Variational graph auto-encoders. *arXiv preprint arXiv:1611.07308*.

Kipf, T. N.; and Welling, M. 2017. Semi-supervised classification with graph convolutional networks. In *ICLR*.

LeCun, Y. ???? The mnist database of handwritten digits. <http://yann.lecun.com/exdb/mnist/>, 1998.

Lyons, M.; Budynek, J.; and Akamatsu, S. 1999. Automatic classification of single facial images. *IEEE transactions on pattern analysis and machine intelligence* 21(12): 1357–1362.

Makhzani, A.; Shlens, J.; Jaitly, N.; Goodfellow, I.; and Frey, B. 2015. Adversarial autoencoders. *arXiv preprint arXiv:1511.05644*.

Nene, S.; Nayar, S.; and Murase, H. 1996. Columbia object image library (coil-20).

Ng, A. Y.; Jordan, M. I.; and Weiss, Y. 2002. On spectral clustering: Analysis and an algorithm. In *Advances in neural information processing systems*, 849–856.

Nie, F.; Wang, X.; and Huang, H. 2014. Clustering and projected clustering with adaptive neighbors. In *Proceedings of the 20th ACM SIGKDD international conference on Knowledge discovery and data mining*, 977–986. ACM.

Niepert, M.; Ahmed, M.; and Kutzkov, K. 2016. Learning convolutional neural networks for graphs. In *International conference on machine learning*, 2014–2023.

Pan, S.; Hu, R.; Long, G.; Jiang, J.; Yao, L.; and Zhang, C. 2018. Adversarially Regularized Graph Autoencoder for Graph Embedding. In *IJCAI*, 2609–2615.

Park, J.; Lee, M.; Chang, H. J.; Lee, K.; and Choi, J. Y. 2019. Symmetric graph convolutional autoencoder for unsupervised graph representation learning. In *Proceedings of the IEEE International Conference on Computer Vision*, 6519–6528.

Peng, X.; Feng, J.; Xiao, S.; Yau, W.-Y.; Zhou, J. T.; and Yang, S. 2018. Structured autoencoders for subspace clustering. *IEEE Transactions on Image Processing* 27(10): 5076–5086.

Perozzi, B.; Al-Rfou, R.; and Skiena, S. 2014. Deepwalk: Online learning of social representations. In *Proceedings of the 20th ACM SIGKDD international conference on Knowledge discovery and data mining*, 701–710. ACM.

Roweis, S. T.; and Saul, L. K. 2000. Nonlinear dimensionality reduction by locally linear embedding. *Science* 290(5500): 2323–2326.

Scarselli, F.; Gori, M.; Tsoli, A. C.; Hagenbuchner, M.; and Monfardini, G. 2008. The graph neural network model. *IEEE Transactions on Neural Networks* 20(1): 61–80.

Shaham, U.; Stanton, K.; Li, H.; Nadler, B.; Basri, R.; and Kluger, Y. 2018. Spectralnet: Spectral clustering using deep neural networks. *arXiv preprint arXiv:1801.01587*.

Tenenbaum, J. B.; Silva, V. D.; and Langford, J. C. 2000. A global geometric framework for nonlinear dimensionality reduction. *Science* 290(5500): 2319–2323.

Wang, C.; Pan, S.; Hu, R.; Long, G.; Jiang, J.; and Zhang, C. 2019. Attributed graph clustering: a deep attentional embedding approach. In *Proceedings of the 28th International Joint Conference on Artificial Intelligence*, 3670–3676. AAAI Press.

Wang, C.; Pan, S.; Long, G.; Zhu, X.; and Jiang, J. 2017. Mgae: Marginalized graph autoencoder for graph clustering. In *Proceedings of the 2017 ACM on Conference on Information and Knowledge Management*, 889–898.

Wang, D.; Cui, P.; and Zhu, W. 2016. Structural deep network embedding. In *Proceedings of the 22nd ACM SIGKDD international conference on Knowledge discovery and data mining*, 1225–1234.

Wang, H.; Wang, J.; Wang, J.; Zhao, M.; Zhang, W.; Zhang, F.; Xie, X.; and Guo, M. 2018. Graphgan: Graph representation learning with generative adversarial nets. In *Thirty-Second AAAI Conference on Artificial Intelligence*, 2508–2515.

Wu, F.; Zhang, T.; Holanda de Souza, A.; Fifty, C.; Yu, T.; and Weinberger, K. Q. 2019. Simplifying graph convolutional networks. *Proceedings of Machine Learning Research* .

Xie, J.; Girshick, R.; and Farhadi, A. 2016. Unsupervised deep embedding for clustering analysis. In *International conference on machine learning*, 478–487.

Xu, K.; Hu, W.; Leskovec, J.; and Jegelka, S. 2019. How powerful are graph neural networks? In *Proc. of ICLR*.

Yang, J.; Parikh, D.; and Batra, D. 2016. Joint unsupervised learning of deep representations and image clusters. In *Proceedings of the IEEE Conference on Computer Vision and Pattern Recognition*, 5147–5156.

Yang, X.; Deng, C.; Zheng, F.; Yan, J.; and Liu, W. 2019. Deep spectral clustering using dual autoencoder network. In *Proceedings of the IEEE Conference on Computer Vision and Pattern Recognition*, 4066–4075.

Zhang, R.; Li, X.; Zhang, H.; and Nie, F. 2019. Deep Fuzzy K-Means with Adaptive Loss and Entropy Regularization. *IEEE Transactions on Fuzzy Systems* 1–1. ISSN 1941-0034. doi:10.1109/TFUZZ.2019.2945232.

Zhang, R.; Nie, F.; Guo, M.; Wei, X.; and Li, X. 2018. Joint Learning of Fuzzy k-Means and Nonnegative Spectral Clustering With Side Information. *IEEE Transactions on Image Processing* 28(5): 2152–2162.

Proof of Theorem 1

Theorem. *The ℓ_2 -norm relaxation of the original problem,*

$$\min_{p(\cdot|v_i)} \sum_{i=1}^n \mathbb{E}_{v_j \sim p(\cdot|v_i)} d_{ij} + \gamma_i \|\mathbf{p}_i\|_2^2, \quad (1)$$

has a k -sparse solution if γ_i satisfies

$$\frac{1}{2}(kd_i^{(k)} - \sum_{v=1}^k d_i^{(v)}) < \gamma_i \leq \frac{1}{2}(kd_i^{(k+1)} - \sum_{v=1}^k d_i^{(v)}). \quad (2)$$

where $d_i^{(v)}$ denotes the v -th smallest value of $\{d_{ij}\}_{j=1}^n$.

Proof. The problem to optimize is equivalent to the following subproblem

$$\min_{p^T \mathbf{1}=1, p \geq 0} \|\mathbf{p} + \frac{\mathbf{d}}{2\gamma}\|_2^2 \quad (3)$$

where the subscript i is ignored. According to the KKT conditions, we have

$$\begin{cases} p_j + \frac{d_j}{2\gamma} - \alpha - \beta_j = 0 \\ \beta_j p_j = 0, \beta_j \geq 0 \\ \sum_{j=1}^n p_j = 1, p_j \geq 0 \end{cases} \Rightarrow p_j = (\alpha - \frac{d_j}{2\gamma})_+. \quad (4)$$

Note that the auxiliary function

$$f(x) = (C_1 - \frac{C_2}{2x})_+, \forall C_2 > 0 \quad (5)$$

is non-decreasing with x . Note that $f(x)$ is strictly increasing when $2x \geq C_2$. If $\alpha \in [\frac{d_1}{2\gamma}, \frac{d_n}{2\gamma}]$, there must exist m that satisfies $\alpha - \frac{d_{m+1}}{2\gamma} \leq 0 < \alpha - \frac{d_m}{2\gamma}$. In this case, \mathbf{p} is m -sparse. According to Eq. (4), we have

$$\alpha = \frac{1}{m} \left(1 + \sum_{j=1}^m \frac{d_j}{2\gamma} \right) \Rightarrow p_j = \frac{1}{m} \left(1 - \frac{\sum_{i=1}^m (d_j - d_i)}{2\gamma} \right)_+ \quad (6)$$

When γ satisfies Eq. (2), we have

$$\frac{1}{m} \left(1 - \frac{\sum_{i=1}^m (d_j - d_i)}{\sum_{i=1}^k (d_k - d_i)} \right)_+ \leq p_j \leq \frac{1}{m} \left(1 - \frac{\sum_{i=1}^m (d_j - d_i)}{\sum_{i=1}^{k+1} (d_{k+1} - d_i)} \right)_+ \quad (7)$$

according to the non-decreasing property of the auxiliary function $f(x)$. If $m > k$, then

$$0 \leq p_m \leq \frac{1}{m} \left(1 - \frac{\sum_{i=1}^m (d_m - d_i)}{\sum_{i=1}^k (d_k - d_i)} \right)_+ \leq 0 \quad (8)$$

Hence, $p_m = 0$ which leads to contradiction. If $m < k$

$$p_{m+1} > \frac{1}{m} \left(1 - \frac{\sum_{i=1}^m (d_{m+1} - d_i)}{\sum_{i=1}^k (d_k - d_i)} \right)_+ > 0 \quad (9)$$

In the first inequality, the equality will never hold due to $2\gamma > \sum_{i=1}^k (d_k - d_i) \geq \sum_{i=1}^k (d_k - d_i)$. Accordingly, \mathbf{p} is at least $(m+1)$ -sparse, which lead to contradiction as well. Therefore, we have $k = m$.

When $(\frac{d_n}{2\gamma}, +\infty)$, it is not hard to verify that $p_m = 0$ which also leads to contradiction. Finally, $\alpha \in (-\infty, \frac{d_1}{2\gamma})$ will never hold due to the constraint $\mathbf{p}^T \mathbf{1} = 1$.

In sum, the theorem is proved. \square

Proof of Theorem 2

Proof of Theorem 2. Without loss of generality, we focus on the connectivity distribution of v and suppose that $p(v_1|v) \geq p(v_2|v) \geq \dots \geq p(v_k|v) > 0 = p(v_{k+1}|v) = \dots = p(v_n|v)$. Let $p_i = p(v_i|v)$ and $q_i = q(v_i|v)$. According to the definitions,

$$\begin{cases} p_i = \frac{d_{k+1}-d_i}{\sum_{j=1}^k (d_{k+1}-d_j)} \\ q_i = \frac{\exp(-\hat{d}_i)}{\sum_{j=1}^n \exp(-\hat{d}_j)}. \end{cases} \quad (10)$$

If for any i , we have $|p_i - q_i| \leq \varepsilon$. Clearly, $p_{k+1} = 0$. Suppose that $q_{k+1} = \tau \leq \varepsilon$. Therefore, we have

$$\begin{aligned} \frac{\exp(-\hat{d}_{k+1})}{\sum_{j=1}^n \exp(-\hat{d}_j)} &= \tau \\ \Leftrightarrow \hat{d}_{k+1} &= \log \frac{1}{\tau} - \log C. \end{aligned} \quad (11)$$

where $C = \sum_{j=1}^n \exp(-\hat{d}_j)$. Combine with the condition, $p_k \geq \sqrt{\varepsilon}$, and we have

$$\begin{aligned} \frac{\exp(-\hat{d}_k)}{\sum_{j=1}^n \exp(-\hat{d}_j)} &\geq p_k - \varepsilon \geq \sqrt{\varepsilon} - \varepsilon \\ \Rightarrow \hat{d}_k &\leq -\log C - \log(\sqrt{\varepsilon} - \varepsilon) \end{aligned} \quad (12)$$

Similarly, since $p_1 \geq 1/k$,

$$\begin{aligned} \frac{\exp(-\hat{d}_1)}{\sum_{j=1}^n \exp(-\hat{d}_j)} &\leq 1 \\ \Rightarrow \hat{d}_1 &\geq -\log C \end{aligned} \quad (13)$$

If we update the connectivity distribution based on $\{\hat{d}_i\}_{i=1}^n$, then for any $i \leq k$,

$$\hat{p}_i = \frac{\hat{d}_{k+1} - \hat{d}_i}{\sum_{j=1}^k (\hat{d}_{k+1} - \hat{d}_j)}. \quad (14)$$

Furthermore, for any $i, j \leq k$,

$$\begin{aligned} |\hat{p}_i - \hat{p}_j| &= \frac{|\hat{d}_j - \hat{d}_i|}{\sum_{j=1}^k (\hat{d}_{k+1} - \hat{d}_j)} \\ &\leq \frac{|\hat{d}_k - \hat{d}_1|}{\sum_{j=1}^k (\hat{d}_{k+1} - \hat{d}_j)} \\ &= \frac{-\log(\sqrt{\varepsilon} - \varepsilon)}{\sum_{j=1}^k (\log \frac{1}{\tau} - \log C - \hat{d}_j)} \\ &\leq \frac{-\log(\sqrt{\varepsilon} - \varepsilon)}{\sum_{j=1}^k (\log \frac{1}{\tau} - \log C - \hat{d}_k)} \\ &\leq \frac{-\log(\sqrt{\varepsilon} - \varepsilon)}{k(\log(\sqrt{\varepsilon} - \varepsilon) - \log \tau)} \\ &= \frac{1}{k} \cdot \frac{\log(\sqrt{\varepsilon} - \varepsilon)}{\log \tau - \log(\sqrt{\varepsilon} - \varepsilon)} \\ &= \frac{1}{k} \cdot \frac{1}{\frac{\log \tau}{\log(\sqrt{\varepsilon} - \varepsilon)} - 1} \\ &\leq \frac{1}{k} \cdot \frac{1}{\frac{\log \varepsilon}{\log(\sqrt{\varepsilon} - \varepsilon)} - 1} \end{aligned} \quad (15)$$

With $\varepsilon \rightarrow 0$, $|\hat{p}_i - \hat{p}_j| \rightarrow 0$.

The proof is easy to extend to other nodes. Hence, the theorem is proved. \square

Proof of Theorem 3

Proof of Theorem 3. The problem,

$$\min_{q(\cdot|v_i)} \sum_{i=1}^n \mathbb{E}_{v_j \sim q(\cdot|v_i)} \hat{d}_{ij} - H_i(v), \quad (16)$$

is equivalent to the following i -th subproblem

$$\begin{aligned} \min_{q_{ij}} \sum_{j=1}^n q_{ij} \hat{d}_{ij} + q_{ij} \log q_{ij} \\ \text{s.t. } \sum_{j=1}^n q_{ij} = 1, q_{ij} > 0 \end{aligned} \quad (17)$$

Similarly, the subscript i is omitted to keep notations uncluttered. The Lagrangian is

$$\mathcal{L} = \sum_{j=1}^n q_j \hat{d}_j + q_j \log q_j + \alpha(1 - \sum_{j=1}^n q_j) + \sum_{j=1}^n \beta_j (-q_j) \quad (18)$$

Then the KKT conditions are

$$\begin{cases} \hat{d}_j + 1 + \log q_j - \alpha - \beta_j &= 0 \\ 1 - \sum_{j=1}^n q_j &= 0 \\ \beta_j q_j &= 0 \\ \beta_j &\geq 0 \end{cases} \quad (19)$$

Due to $q_j > 0$, $\beta_j = 0$. Use the first line, we have

$$q_j = \exp(\alpha - \hat{d}_j - 1) \quad (20)$$

Dataset	λ	k_0	γ	t_i	k_m	T	struct
Text	0.01	30	$5 * 10^{-3}$	150	$\lfloor \frac{n}{c} \rfloor$	10	$d\text{-}256\text{-}64$
20news	0.1	20	10^{-3}	200	$\lfloor \frac{n}{2c} \rfloor$	10	$d\text{-}256\text{-}64$
Isolet	0.1	20	10^{-3}	200	$\lfloor \frac{n}{c} \rfloor$	5	$d\text{-}256\text{-}64$
PALM	10	10	10^{-3}	50	$\lfloor \frac{n}{c} \rfloor$	10	$d\text{-}256\text{-}64$
UMIST	1	5	10^{-3}	50	$\lfloor \frac{n}{c} \rfloor$	10	$d\text{-}256\text{-}64$
COIL20	1	5	10^{-2}	100	$\lfloor \frac{n}{2c} \rfloor$	10	$d\text{-}256\text{-}64$
JAFFE	10^{-3}	5	10^{-2}	20	$\lfloor \frac{n}{c} \rfloor$	10	$d\text{-}256\text{-}64$
USPS	10^{-2}	5	5×10^{-3}	150	$\lfloor \frac{n}{c} \rfloor$	10	$d\text{-}128\text{-}64$
MNIST	10^{-2}	5	10^{-3}	200	$\lfloor \frac{n}{2c} \rfloor$	10	$d\text{-}256\text{-}64$

Table 3: λ : local information; k_0 : initial sparsity; γ : learning rate; λ : regularization coefficient; t_i : number of iterations to update GAE; struct: Neurons of each layer used in AdaGAE.

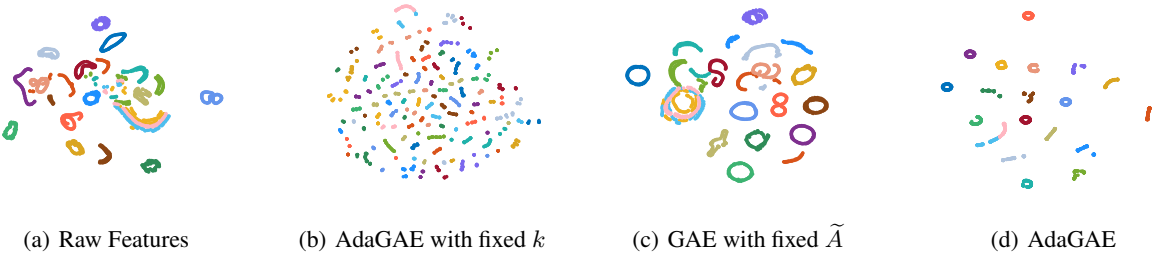


Figure 4: t-SNE visualization on COIL20.

Name	# Features	# Size	# Classes
Text	7511	1946	2
20news	8014	3970	4
Isolet	617	1560	26
PALM	256	2000	100
UMIST	1024	575	20
JAFFE	1024	213	10
COIL20	1024	1440	20
USPS	256	1854	10
MNIST	784	10000	10

Table 4: Information of Datasets

Combine it with the second line and we have

$$\exp(\alpha) \sum_{j=1}^n \exp(-\hat{d}_j - 1) = 1 \quad (21)$$

Furthermore, we have

$$q_j = \frac{\exp(-\hat{d}_j - 1)}{\sum_{j=1}^n \exp(-\hat{d}_j - 1)} = \frac{\exp(-\hat{d}_j)}{\sum_{j=1}^n \exp(-\hat{d}_j)} \quad (22)$$

With $\hat{d}_{ij} = \|z_i - z_j\|_2$, the theorem is proved. \square

Proof of Theorem 4

It should be pointed out that the proof imitates the corresponding proof in (Wu et al. 2019). Analogous to Lemma 3

in (Wu et al. 2019), we first give the following lemma without proof,

Lemma 1. *Let $\alpha_1 \leq \alpha_2 \leq \dots \leq \alpha_n$ be eigenvalues of $\hat{D}^{-\frac{1}{2}} \hat{A}' \hat{D}^{-\frac{1}{2}}$ and $\beta_1 \leq \beta_2 \leq \dots \leq \beta_n$ be eigenvalues of $\hat{D}'^{-\frac{1}{2}} \hat{A}' \hat{D}'^{-\frac{1}{2}}$. The following inequality always holds*

$$\alpha_1 \geq \frac{\beta_1}{1 + \min \frac{\hat{A}_{ii}}{\hat{D}'_{ii}}}, \alpha_n \leq \frac{1}{1 + \max \frac{\hat{A}_{ii}}{\hat{D}'_{ii}}} \quad (23)$$

The proof of Theorem 4 is apparent according to Lemma 3 provided in (Wu et al. 2019).

Proof of Theorem 4. Let $M = \text{diag}(\hat{A})$ and we have

$$\begin{aligned} \lambda_n &= \max_{\|\mathbf{x}\|=1} \mathbf{x}^T (I - \hat{D}^{-\frac{1}{2}} M \hat{D}^{-\frac{1}{2}} - \hat{D}^{-\frac{1}{2}} \hat{A}' \hat{D}^{-\frac{1}{2}}) \mathbf{x} \\ &\leq 1 - \min \frac{\hat{A}_{ii}}{\hat{D}'_{ii} + \hat{A}_{ii}} - \alpha_1 \\ &\leq 1 - \min \frac{\hat{A}_{ii}}{\hat{D}'_{ii} + \hat{A}_{ii}} - \frac{\beta_1}{1 + \min \frac{\hat{A}_{ii}}{\hat{D}'_{ii}}} \\ &\leq 1 - \frac{\beta_1}{1 + \min \frac{\hat{A}_{ii}}{\hat{D}'_{ii}}} \\ &\leq 1 - \beta = \lambda'_n \end{aligned}$$

\square

Experimental Details

Datasets

For all datasets, we simply rescale features into $[0, 1]$. All datasets are downloaded from <http://www.escience.cn/people/fpnie/index.html> and <http://yann.lecun.com/exdb/mnist/>. The concrete information of them is summarized in Table 4.

Experimental Setting

The exact values of AdaGAE in our experiments are reported in Table 3. Note that the increment t is defined as $\frac{k_m - k_0}{T}$.

To use Ratio Cut and Normalized Cut, we construct the graph via Gaussian kernel, which is given as

$$w_{ij} = \frac{\exp(-\frac{\|\mathbf{x}_i - \mathbf{x}_j\|_2}{\sigma})}{\sum_{j \in \mathcal{N}_i} \exp(-\frac{\|\mathbf{x}_i - \mathbf{x}_j\|_2}{\sigma})} \quad (24)$$

where \mathcal{N}_i represents m -nearest neighbors of sample \mathbf{x}_i . m is searched from $\{5, 10\}$ and σ is searched from $\{10^{-3}, 10^{-2}, \dots, 10^3\}$. The maximum iterations of GAE with fixed \tilde{A} is set as 200.

Codes of competitors are implemented under MATLAB 2019a, while codes of AdaGAE are implemented under pytorch-1.3.1-gpu. We run all experiments on a Windows PC with 8 i7 cores and a NVIDIA GeForce 1660 (6GB).

Another Visualization

The t-SNE visualization of various methods on COIL20 are shown in Figure 4. From the figure, we can find that the update of k avoid the collapse caused by the adaptive construction of the graph.